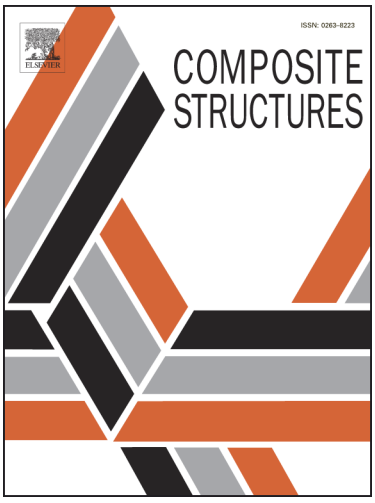

On the dynamics of FG-GPLRC sandwich cylinders based on an unconstrained higher-order theory

Arameh Eyvazian, Tamer A. Sebaey, Krzysztof Kamil Żur, Afrasyab Khan, Hexin Zhang, Simon H. F. Wong

PII: S0263-8223(21)00339-1
DOI: https://doi.org/10.1016/j.compstruct.2021.113879
Reference: COST 113879

To appear in: *Composite Structures*

Please cite this article as: Eyvazian, A., Sebaey, T.A., Żur, K.K., Khan, A., Zhang, H., F. Wong, S.H., On the dynamics of FG-GPLRC sandwich cylinders based on an unconstrained higher-order theory, *Composite Structures* (2021), doi: https://doi.org/10.1016/j.compstruct.2021.113879

On the dynamics of FG-GPLRC sandwich cylinders based on an unconstrained higher-order theory

Arameh Eyvazian[1], Tamer A. Sebaey[2,3], Krzysztof Kamil Żur [4], Afrasyab Khan [5], Hexin Zhang [6], Simon H. F. Wong [7]

Abstract

In the present paper, a novel unconstrained higher-order theory (UCHOT) is applied to analyse the free vibration of cylindrical sandwich shells with nanocomposite face sheets reinforced with graphene platelets. UCHOT considers the shear and thickness deformations. It is assumed that the cylinder includes a soft core which embedded between functionally graded graphene platelets reinforced composites (FG-GPLRC). FG-GPLRC face sheet consists of several laminas that the GPL weight fraction is modified layer to layer based on the various functionally graded (FG) patterns. The Winkler-Pasternak elastic foundation is located at the inner surface of the shell. Highly coupled motion equations are solved by a semi-analytical approach. This approach is blended of the generalized differential quadrature and trigonometric expansion (TE-GDQ) methods. Solving the obtained eigenvalue problem, corresponding frequencies to the cylindrical sandwich shell are achieved. In the results part, comparison studies are carried out to indicate the validity and performance of the selected theory and solution method. Afterward, some parametric results are demonstrated to investigate the impacts of shell theory order, geometrical parameters, FG model, elastic foundation parameters, and boundary conditions on the frequency response of the mentioned structure.

Keywords: Frequency Analysis; Graphene Platelets; Sandwich Cylindrical Shell; Unconstrained Higher-Order Plate Theory (UCHOT); Elastic Foundation.

1 Introduction

1.1 Background

Sandwich structures are important class of structures because of their preferable properties such as great bending stiffness and low specific weight with application in

[1]Department of Mechanical and Industrial Engineering, College of Engineering, Qatar University, P.O. Box 2713, Doha, Qatar. Email: eyvazian@qu.edu.qa. Corresponding author

[2]Engineering Management Department, College of Engineering, Prince Sultan University, Riyadh, Saudi Arabia.

[3]Mechanical Design and Production Department, Faculty of Engineering, Zagazig University, P.O. Box 44519, Zagazig, Sharkia, Egypt.

[4]Faculty of Mechanical Engineering, Bialystok University of Technology, Bialystok, 15-351, Poland. Co corresponding author

[5]Institute of Engineering and Technology, Department of Hydraulics and Hydraulic and Pneumatic Systems, South Ural State University, Lenin Prospect 76, Chelyabinsk, 454080, Russian Federation.

[6]School of Engineering and the Built Environment, Edinburgh Napier University, 10 Colinton Road, Edinburgh, Scotland, UK, EH10 5DT

[7]Department of Construction Technology and Engineering, Technological Higher Education Institute of Hong Kong, 20A Tsing Yi Road, Tsing Yi Island, New Territories, Hong Kong.

medical, aircraft and aerospace space vehicles and portage systems [1,2]. One of the most widely used class of this structures can be constituted of a placed homogeneous soft core between two face sheets made of isotropic material [3], fiber-reinforced composites [4,5], carbon nanotube [6,7], or functionally graded materials [8–10]. Owing to ultramodern electrical, thermal and mechanical characteristics of nanofillers, they are largely tested to augment the polymer composites, instead of usual elongated fibers. Beside to uniform prorating, nanocomposites can also be functionally graded (FG) reinforced [11]. Graphene has a greater ability to react with the matrix than other nano-amplifiers due to their flat appearance, so its application will be more effective than other nanofillers [12–16]. Due to chemical properties, the dispensation of graphene sheets to a matrix causes them to react with together, which ultimately form graphene platelets (GPLs) [17]. So-called nanocomposites reinforced with GPLs are called FG-GPLRC. The employing of this type of modern nanocomposites as face sheets in sandwiches can enormously better their vibrational response [18].

1.2 Literature survey

Latterly, large number of experimental and analytical articles have been accomplished regarding the vibrational behavior of reinforced structures by GPLs. Rafiee et al. [17] discovered that the improved elastic stiffness and strength due to appending 0.1 w.t.% (weight fraction) of GPLs, is equivalent to adding 1 w.t.% of CNTs. Besides, King et al. [19] manufactured a graphene reinforced composite (GRC) structure and showed that enhancing 6.0 w.t.% graphene could magnify the elasticity modulus from 2.72 GPa to 3.36 GPa. Fang et al. [20] showed that synthesis of 0.9 wt.% graphene sheets to polystyrene may eventuate 57.2 % increment of the Young modulus. Some analysis depicted that the exerting graphene either in sheets or platelets types will amplify the natural frequency of the plates and shells in comparison of the graphene-free ones. For instance, Song et al. [21] ascertained that employing just 1.2 wt.% graphene will boost the natural frequencies of the rectangular plate about 160 %. Chandra et al. [22] scrutinized the outcomes of several models of nanocomposite manufacturing on their vibration behavior and discussed on the significant role of graphene sheets sizes in increment of the natural frequency. However, it should be attended that, graphene weight fraction cannot be exceedingly increased, because excessive weight fraction of graphene nanofillers causes an unpleasant results [23].

Kitipornchai et al. [24] perused the free vibration of FG-GPLRC beams considering the impact of the porosity and GPLs stepwise distribution along the beam thickness. In this study, the porosity is considered based on the closed-cell model according to the Gaussian random law. In addition, the conventional Ritz method is used. It is evidenced that the beam natural frequency can be elevated by the variation of distribution model of porosity and GPLs. Dynamic response of edge-cracked nanocomposite beams reinforced with GPLs was analyzed by Song et al. [25]. The rested beam on a two parameter elastic foundation was investigated using thr GDQ tool. The influence of dielectric permittivity on the forced vibration of FG-GPLRC beams was researched by Wang et al. [26]. Barati and Shahverdi [27] proffered the finite element method to examine the force vibration of FG-GPLRC elastic beam. A recent refined shear deformation theory was engaged to develop the formulation. An investigation about the dynamic response of a FG-GPLRC beam was carried out by Wang et al. [28]. It was assumed that the beam was exposed to two subsequent movable masses. It should be mentioned that the Navier solution was

implemented to adopt the response of higher-order shear deformation beam. Li et al. [29] examined the primary and secondary resonances based on the geometrically nonlinear assumptions for FG-GPLRC beams. Galerkin's method was used to this problem. Feng et al. [30] investigated the effect of porosity on the large amplitude free oscillation of the GPL-based nanocomposite beams.

Frequency research was produced for the nanocomposite rectangular plates with inserting the porosity and GPL nanofillers by Yang et al. [31]. The calculated outcomes by means of the Chebyshev-Ritz procedure shows that the X-model of functionally graded material makes a plate with extra natural frequencies. Reddy et al. [32] convinced various boundary conditions around the FG-GPLRC rectangular plate for a free vibration study. Zhao et al. [33] acceded the greater natural frequencies utilizing the amplified trapezoidal plates by GPLs. Free vibration of FG-GPLRC quadrilateral plates imposing the modified Halpin-Tsai micromechanical rule is scrutinized by Guo et al. [34]. Gholami and Ansari [35] analyzed the free vibration of FG-GPLRC plates utilizing the variational differential quadrature (VDQ) technique. In this research, the free vibration was investigated for the mechanically pre- or post-buckled plates. Malekzadeh et al. [36] presented the effect of piezoelectric layers attached to the FG-GPLRC eccentric annular plates on their free vibrations implementing the GDQ method based on the polar coordinate mapping. Saidi et al. [37] surveyed the authority of GPLs reinforcement, piezoelectric plies, and porous cells on the flutter aerodynamic pressure and free vibration response of plates. As a further case of vibration control, Salim et al. [38] controlled the vibrations of FG-GPLRC plate applying two piezoelectric layers based on the velocity feedback control. This research was done using an element free method based on the improved moving least-squares Ritz associated with higher-order shear deformation theory. The effects of thermal environment and axial loading on the axisymmetric free vibration of annular plates were analyzed by Wang et al. [39]. The extracted motion equations of higher-order shear deformable plate were solved by means of GDQ tool. Gholami et al. [40, 41] bringed up the VDQ method to research the geometrically nonlinear free and forced vibrations of FG-GPLRC rectangular plates considering the third-order shear deformation assumptions. Liu et al. [42] analyzed the three-dimensional free oscillation of annular plates utilizing the state-space based GDQ technique. Dong et al. [43, 44] analyzed the asymmetric linear and non-linear free vibration response of FG-GPLRC cylindrical shells with spinning motion. Analytically and Galerkin's techniques are in order utilized to obtain the response of governing motion equations related to small and large amplitude vibrations. First-order shear deformation is applied to estimate the displacement field. Usage of porosity in controlling the natural frequencies behavior of FG-GPLRC cylindrical shells is presented by Barati and Zenkour [45]. The dynamic response obtained of the impulse loaded FG-GPLRC cylindrical shell has been investigated by Heydarpour et al. [46] adopting the DQ-Heaviside-NURBS combination approach. Wang et al. [47] inspected the GPL trigonometric dispersal effect on the large amplitude vibration of hollow cylinders. metal foam is selected as the matrix material. Niu et al. [48] employed the Chebyshev-Ritz technique to evaluate the natural frequency response of revolving pretwisted nanocomposite cylindrical panels reinforced by GPL. Wang et al. [49] showed a comprehensive research on the free vibration of FG-GPLRC shallow doubly curved panels. Bidzard et al. [50] investigated vibration demeanor of FG-GPLRC toroidal panels with edges that are resistant to elastic rotation. Liu et al. [51] analytically investigated the three dimensional free vibration of thin, moderately thick, and thick hollow cylinders. It is assumed that the structure is initially stressed.

There are many approach to obtain the structure frequencies. Some of them are based on the energy approach [52–54]. Others are applied to the motion equations in the strong form [55]. These types of solutions are generally in the three categories: nodal, element, and meshless [56] methods. One of the most implemented nodal methods are generalized differential quadrature method. The GDQ is a simple and efficiency method which divide the solution domain in some nodal points. More details are demonstrated in the solution section [57].

1.3 Voids in the literature

Although theoretical research on the GPL-reinforced nanocomposite structures are rich, articles about the vibration of sandwich structures with GPL-reinforced skins are limited. Nematollahi et al. [58] gave a nonlinear free vibration study on the sandwich beams with FG-GPLRC skins. The third-order shear deformation theory was utilized in formulation of governing equations. Applying the transformed differential quadrature method, Liang et al. [59] demonstrated the vibration behavior study of shear deformable trapezoidal sandwich plate consists of a porous core with the outer FG-GPLRC surface sheets. Mohseni and Shakouri [60] investigated the free vibration of sandwich plates consist of the middle viscoelastic core embedded by GPL reinforced nanocomposites layers on its surfaces.

Based on the above-reviewed studies, it is detected that published investigations on the sandwiches incorporating the FG-GPLRC surfaces are all based on the plate/shell theories and do not take into account the thickness deformation of the structure. Usually, only shear deformations of structures were taken into account. However, there is not even an article on the vibrations of a cylindrical sandwich shell with FG-GPLRC layers. The current research examines the free vibration of FG-GPLRC cylindrical sandwich shells based on a novel unconstrained higher-order theory. The utilized shell theory considered shear deformations, rotary inertias and also thickness variations. The effective of Young's modulus for nanocomposite face sheets is obtained based on the Halpin-Tsai homogenization model. The governing motion equations are solved implementing a semi-analytical approach based on the trigonometric expansion and generalized differential quadrature methods. It is assumed that the shell is on the Winkler-Pasternak elastic foundation. The parametric studies are demonstrated to obtain the convergence criterion for order of UCHOT. In addition, the effects of various boundary conditions, geometrical, material factors, and also, a two-parameter elastic foundation on the natural frequencies of the sandwich shell are investigated.

2 Geometric and material characteristics of sandwich cylindrical shell

A circular cylindrical sandwich shell with a desired total thickness h, mean radius R and length L is considered. It is assumed that two FG-GPLRC face sheets surround a soft core. Thickness of each FG-GPLRC face sheet is indicated by h_f and core thickness is h_c ($h = h_c + 2h_f$). A cylindrical coordinate is assumed on the middle surface of shell (x, θ, z). z is measured from the middle surface and changes from $-h/2$ to $h/2$ which is positive outward as depicted in Fig. 1.

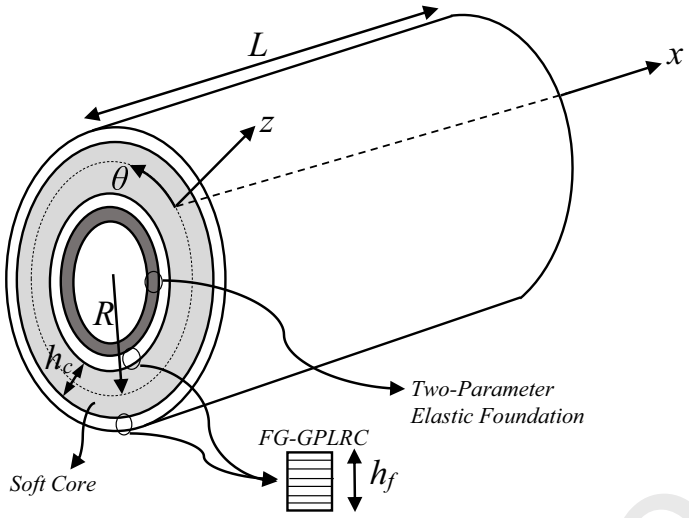

Figure 1: A schematic figure of the FG-GPLRC sandwich hollow cylinder on the elastic foundation.

The sandwich cylinder is made of perfectly connected laminas. Each ply of FG-GPLRC is made of composition of GPL reinforcements and isotropic matrix. In addition, GPLs are randomly oriented and uniformly distributed; hence GPL weight fraction should be considered as constant in the total of a ply. Besides, nanofillers weight fraction varies from layer-to-layer based on the five functionally graded patterns as shown in Fig. 2.

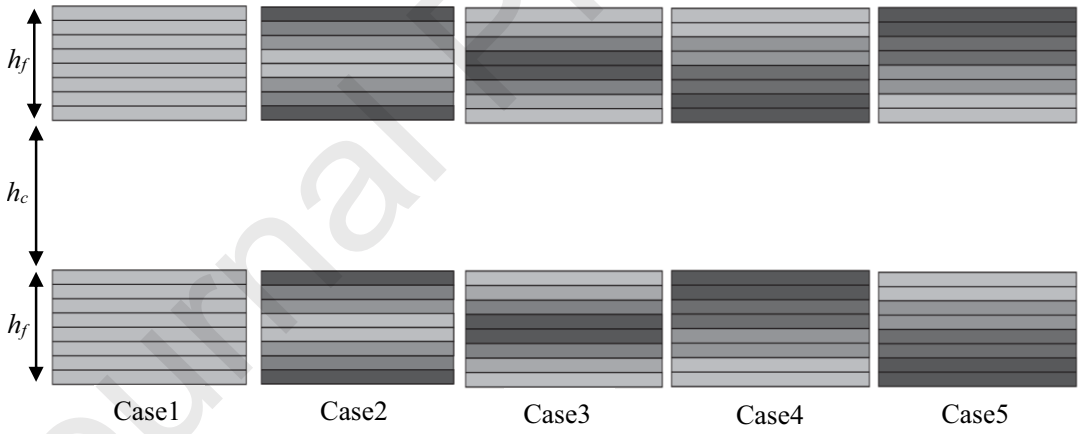

Figure 2: Functionally graded distributions.

Number of layers for each FG-GPLRC face sheet is even and indicated by N_L. It should be mentioned that the number of plies in the upper and lower face sheets is equal. Several step layerwise for GPL weight fraction changes are supposed for the top and bottom face sheets. The volume fraction of each ply $V_{GPL}^{(k)}$ based on the various functionally graded models are calculated in Table (1) [36, 61].

The total volume fraction of GPLs in each face sheet V_{GPL}^{*} is computed in terms of

Table 1: FG GPL distribution models along the top and bottom composite thickness.

FG name	top GPLRC face sheet	bottom GPLRC face sheet
Case1: $\binom{U}{U}$	$V_{GPL}^{(k)} = V_{GPL}^{*}$	$V_{GPL}^{(k)} = V_{GPL}^{*}$
Case2: $\binom{X}{X}$	$V_{GPL}^{(k)} = 2V_{GPL}^{*}\lvert 2k - N_L - 1\rvert / N_L$	$V_{GPL}^{(k)} = 2V_{GPL}^{*}\lvert 2k - N_L - 1\rvert / N_L$
Case3: $\binom{O}{O}$	$V_{GPL}^{(k)} = 2V_{GPL}^{*}(1 - \lvert 2k - N_L - 1\rvert / N_L)$	$V_{GPL}^{(k)} = 2V_{GPL}^{*}(1 - \lvert 2k - N_L - 1\rvert / N_L)$
Case4: $\binom{\Lambda}{V}$	$V_{GPL}^{(k)} = V_{GPL}^{*}(2(N_L - k) + 1)/N_L$	$V_{GPL}^{(k)} = V_{GPL}^{*}(2k - 1)/N_L$
Case5: $\binom{V}{\Lambda}$	$V_{GPL}^{(k)} = V_{GPL}^{*}(2k - 1)/N_L$	$V_{GPL}^{(k)} = V_{GPL}^{*}(2(N_L - k) + 1)/N_L$

GPLs weight fraction W_{GPL}

$$V_{GPL}^{*} = \frac{W_{GPL}}{W_{GPL} + \left(\frac{\rho_{GPL}}{\rho_m}\right)(1 - W_{GPL})} \tag{1}$$

The mass density of the constituents are presented by ρ_m and ρ_{GPL}. Halpin-Tsai's micromechanical rule as a second-order correlation homogenization rule which is considered as the geometry and size of reinforcements in obtaining the effective material properties [62,63] is used. Accordingly, Young's modulus of each ply may be attained by utilizing the Halpin-Tsai micromechanical rule as

$$E^{(k)} = \frac{3}{8}\frac{1 + \xi_L \eta_L V_{GPL}^{(k)}}{1 - \eta_L V_{GPL}^{(k)}} \times E_m + \frac{5}{8}\frac{1 + \xi_T \eta_T V_{GPL}^{(k)}}{1 - \eta_T V_{GPL}^{(k)}} \times E_m \tag{2}$$

in which, two ancillary parameters η_L and η_T in Eq. (2) are given below

$$\eta_L = \frac{\left(\frac{E_{GPL}}{E_m}\right) - 1}{\left(\frac{E_{GPL}}{E_m}\right) + \xi_L}, \quad \eta_T = \frac{\left(\frac{E_{GPL}}{E_m}\right) - 1}{\left(\frac{E_{GPL}}{E_m}\right) + \xi_T} \tag{3}$$

where E_m and E_{GPL} present the Young modulus of the isotropic matrix and GPLs, respectively. The geometric coefficients of used amplifications are explained in terms of the GPLs thickness t_{GPL}, width b_{GPL}, and length a_{GPL} as follows

$$\xi_L = 2\left(\frac{a_{GPL}}{t_{GPL}}\right), \quad \xi_T = 2\left(\frac{b_{GPL}}{t_{GPL}}\right) \tag{4}$$

Due to the small distinction between the density and the Poisson's ratio of graphene and polymer used, Voigt's model is satisfactory to extract the equivalent magnitude of these parameters. These amounts can be calculated by

$$\begin{aligned} \rho^{(k)} &= \rho_{GPL} V_{GPL}^{(k)} + \rho_m V_m^{(k)} \\ \nu^{(k)} &= \nu_{GPL} V_{GPL}^{(k)} + \nu_m V_m^{(k)} \end{aligned} \tag{5}$$

In Eq. (5), the subscripts m and GPL corresponds to the matrix and graphene platelets, respectively. Also, $V_m = 1 - V_{GPL}$ is the isotropic polymer volume fraction. It should be attended that the captured soft core is considered isotropic and homogeneous. Its Young's modulus, Poisson's ratio and mass density are demonstrated by E_c, ν_c, and ρ_c, respectively. Since it is used a soft core surrounded by two FG-GPLRC face sheet, the total layers of sandwich which is displayed by N_t is $N_t = 2N_L + 1$.

3 Basic formulation

In the mechanical examinations of thick sandwich structures, choosing a suitable theory in light of the accuracy of final results seems to be notable. Love first presented the theory of shells based on Euler's classical theory of beams [64]. This theory merely considered the effect of bending and stretching of the plates/shells. Reissner extended the previous theory by considering the influence of shear deformations [65]. This theory is based on the Timoshenko theory for beams and is known as the first-order shear deformation theory (FSDT). Next, Reddy reported a third-order theory for in-plane displacements to apply the impact of free stress condition on the structure surfaces in mechanical behaviors [66]. Other higher order theories can be viewed in the articles [67,68]. All of these theories for formulating the plates and shells behavior, although suitable for thicker structures, respectively, did not take into account changes of the thickness, and the alone way to apply this effect was to employing the three-dimensional theory of elasticity. Matsunaga [69], with expansion of displacements in every direction to high and desired orders, was able to investigate the effects of thickness modification without implementing the three-dimensional elasticity approach. He implemented this theory to investigate the free vibrations of cylindrical shells and extracted the natural frequencies of these structures with arbitrary thickness [70,71]. Sahraee et al. [72] analyzed the free vibration of thick beam on the elastic foundation using the Matsunaga theory. Javani et al. [73] developed this theory to investigate the free vibration of a deep FGM arches. They called Matsunaga's theory unconstrained higher-order theory (UCHOT). UCHOT is based on the expanding the displacement components to a higher-order of thickness direction. Therefore, unlike other theories in the open literature, this theory considers the effect of thickness changes in the formulation in addition to the effect of shear deformations. The election of the order for this theory is optional and is therefore called the unconstrained theory. Based on this theory, the displacement field of a circular cylinder can be defined as

$$\begin{aligned} u(x,\theta,z,t) &= \sum_{i=0}^{M} z^i u^i(x,\theta,t) \\ v(x,\theta,z,t) &= \sum_{i=0}^{M} z^i v^i(x,\theta,t) \\ w(x,\theta,z,t) &= \sum_{j=0}^{M-1} z^j w^j(x,\theta,t) \end{aligned} \tag{6}$$

u, v, and w indicate the displacements of an arbitrary point of sandwich plate in the meridional, tangential, and thickness directions, respectively. The order of theory is depicted by M. In addition, t represents the time variable. It should be noted that the order of transverse displacement w in this theory is one unit less than the order of expanding of in-plane displacements. The three-dimensional strains related to the UCHOT can be defined as follow

$$
\begin{aligned}
\varepsilon_{xx} &= \sum_{i=0}^{M} z^i u^i_{,x} \\
\varepsilon_{\theta\theta} &= \frac{1}{R(1+z/R)} \left(\sum_{i=0}^{M} z^i v^i_{,\theta} + \sum_{j=0}^{M-1} z^j w^j \right) \\
\varepsilon_{zz} &= \sum_{j=0}^{M-1} z^j_{,z} w^j \\
\gamma_{\theta z} &= \sum_{i=0}^{M} z^i_{,z} v^i + \frac{1}{R(1+z/R)} \left(\sum_{j=0}^{M-1} z^j w^j_{,\theta} - \sum_{i=0}^{M} z^i v^i \right) \\
\gamma_{xz} &= \sum_{i=0}^{M} z^i_{,z} u^i + \sum_{j=0}^{M-1} z^j w^j_{,x} \\
\gamma_{x\theta} &= \frac{1}{R(1+z/R)} \sum_{i=0}^{M} z^i u^i_{,\theta} + \sum_{i=0}^{M} z^i v^i_{,x}
\end{aligned} \tag{7}
$$

It is notable that the trapezoidal shape parameter $(1+z/R)$ is considered to achieve more accurate result for free vibration of thick cylindrical shell. $\varepsilon_{xx}, \varepsilon_{\theta\theta}, \varepsilon_{zz}$ show the normal strains in the length, circumferential, and thickness directions. Moreover, $\gamma_{\theta z}, \gamma_{xz}, \gamma_{x\theta}$ depict the shear strain components. Subscript comma shows the partial derivatives with respect to ulterior letter. Considering the Hooke's law, the stresses and strains of the sandwich elastic media are related by linear relationships. Three-dimensional type of this law is represented below for every layer of sandwich.

$$
\begin{Bmatrix} \sigma_{xx} \\ \sigma_{\theta\theta} \\ \sigma_{zz} \\ \sigma_{\theta z} \\ \sigma_{xz} \\ \sigma_{x\theta} \end{Bmatrix}^{(k)} = \begin{bmatrix} E_1^{(k)} & E_2^{(k)} & E_2^{(k)} & 0 & 0 & 0 \\ E_2^{(k)} & E_1^{(k)} & E_2^{(k)} & 0 & 0 & 0 \\ E_2^{(k)} & E_2^{(k)} & E_1^{(k)} & 0 & 0 & 0 \\ 0 & 0 & 0 & E_3^{(k)} & 0 & 0 \\ 0 & 0 & 0 & 0 & E_3^{(k)} & 0 \\ 0 & 0 & 0 & 0 & 0 & E_3^{(k)} \end{bmatrix} \begin{Bmatrix} \varepsilon_{xx} \\ \varepsilon_{\theta\theta} \\ \varepsilon_{zz} \\ \gamma_{\theta z} \\ \gamma_{xz} \\ \gamma_{x\theta} \end{Bmatrix} \tag{8}
$$

where E_1, E_2, E_3 refer to elastic parameters devoted to each layer and are defined as

$$
\begin{aligned}
E_1^{(k)} &= \frac{E^{(k)}(1-\nu^{(k)})}{(1+\nu^{(k)})(1-2\nu^{(k)})} \\
E_2^{(k)} &= \frac{E^{(k)}\nu^{(k)}}{(1+\nu^{(k)})(1-2\nu^{(k)})} \\
E_3^{(k)} &= \frac{E^{(k)}}{2(1+\nu^{(k)})}
\end{aligned} \tag{9}
$$

It was mentioned that E and ν represent the Young modulus and Poisson's ratio.

4 Governing equations

Implementing Hamilton's principle, the equations of motion are derived. This rule expresses

$$\int_{t_1}^{t_2}(\delta T-\delta V-\delta U)dt=0 \tag{10}$$

δU is the strain energy variation, δT indicates the kinetic energy variation and δV is the variation of work done by the Winkler-Pasternak foundation on the inner surface of shell. This statements for UCHOT-based cylindrical shells may be obtained by

$$\begin{aligned}
\delta U &= \int_0^{2\pi}\int_0^{L}\int_{-0.5h}^{+0.5h}\sigma_{ij}^{(k)}\delta\varepsilon_{ij}R(1+\frac{z}{R})\,dz\,dx\,d\theta \qquad i,j=x,\theta,z\\
\delta V &= \int_0^{2\pi}\int_0^{L}\left\{k_w w|_{z=-h/2}-k_g(w_{,xx}|_{z=-h/2}+\frac{1}{R^2}w_{,\theta\theta}|_{z=-h/2})\right\}\delta w|_{z=-h/2}R(1+\frac{z}{R})|_{z=-h/2}\,dx\,d\theta\\
\delta T &= \int_0^{2\pi}\int_0^{L}\int_{-0.5h}^{+0.5h}\rho^{(k)}\left(\dot{u}\delta\dot{u}+\dot{v}\delta\dot{v}+\dot{w}\delta\dot{w}\right)R(1+\frac{z}{R})\,dz\,dx\,d\theta
\end{aligned} \tag{11}$$

Substituting Eq. (11) into Eq. (10) and using the conventional variational technique, the motion equations of cylindrical sandwich shell integrated with FG-GPLRC surface sheets are acquired in terms of stress resultants as

$$\begin{aligned}
&\delta u^i \quad : \quad N^i_{xx,x}+\frac{1}{R}N^i_{\theta x,\theta}-Q^i_{xz}=\sum_{l=0}^{M}I_{il}\ddot{u}^l, \qquad i=0,...,M,\\
&\delta v^i \quad : \quad \frac{1}{R}N^i_{\theta\theta,\theta}+N^i_{x\theta,x}-Q^i_{\theta z}+\frac{1}{R}\bar{Q}^i_{\theta z}=\sum_{l=0}^{M}I_{il}\ddot{v}^l, \qquad i=0,...,M,\\
&\delta w^j \quad : \quad \bar{Q}^j_{xz,x}+\frac{1}{R}\bar{Q}^j_{\theta z,\theta}-N^j_{zz}-\frac{1}{R}N^j_{\theta\theta}\\
&-\sum_{l=0}^{M-1}(-h/2)^{j+l}(1-\frac{h}{2R})\left\{k_w w^l-k_g(w^l_{,xx}+\frac{1}{R^2}w^l_{,\theta\theta})\right\}=\sum_{l=0}^{M-1}I_{jl}\ddot{w}^l, \qquad j=0,...,M-1
\end{aligned} \tag{12}$$

where stress resultants are defined as

$$\begin{aligned}
(N^i_{xx},N^i_{\theta\theta},N^i_{zz}) &= \sum_{k=1}^{N_t}\int_{z_k}^{z_{k+1}}(\sigma^{(k)}_{xx}z^i(1+z/R),\sigma^{(k)}_{\theta\theta}z^i,\sigma^{(k)}_{zz}z^i_{,z}(1+z/R))dz\\
(N^i_{\theta x},N^i_{x\theta}) &= \sum_{k=1}^{N_t}\int_{z_k}^{z_{k+1}}(\sigma^{(k)}_{x\theta}z^i,\sigma^{(k)}_{x\theta}z^i(1+z/R))dz\\
(\bar{Q}^i_{xz},Q^i_{xz}) &= \sum_{k=1}^{N_t}\int_{z_k}^{z_{k+1}}(\sigma^{(k)}_{xz}z^i(1+z/R),\sigma^{(k)}_{xz}z^i_{,z}(1+z/R))dz\\
(\bar{Q}^i_{\theta z},Q^i_{\theta z}) &= \sum_{k=1}^{N_t}\int_{z_k}^{z_{k+1}}(\sigma^{(k)}_{\theta z}z^i,\sigma^{(k)}_{\theta z}z^i_{,z}(1+z/R))dz
\end{aligned} \tag{13}$$

Substituting Eq. (8) into Eq. (13), these expressions can be written in terms of displacements

$$
\begin{aligned}
N^i_{xx} &= \sum_{l=0}^{M}\left\{C^{x11}_{il}u^l_{,x}+\frac{1}{R}C^{x12}_{il}v^l_{,\theta}\right\}+\sum_{l=0}^{M-1}\left\{\frac{1}{R}C^{x12}_{il}w^l+C^{x13}_{il}w^l\right\}\\
N^i_{\theta\theta} &= \sum_{l=0}^{M}\left\{C^{\theta21}_{il}u^l_{,x}+\frac{1}{R}C^{\theta22}_{il}v^l_{,\theta}\right\}+\sum_{l=0}^{M-1}\left\{\frac{1}{R}C^{\theta22}_{il}w^l+C^{\theta23}_{il}w^l\right\}\\
N^i_{zz} &= \sum_{l=0}^{M}\left\{C^{z31}_{il}u^l_{,x}+\frac{1}{R}C^{z32}_{il}v^l_{,\theta}\right\}+\sum_{l=0}^{M-1}\left\{\frac{1}{R}C^{z32}_{il}w^l+C^{z33}_{il}w^l\right\}\\
N^i_{\theta x} &= \sum_{l=0}^{M}\left\{\frac{1}{R}C^{x\theta11}_{il}u^l_{,\theta}+C^{x\theta12}_{il}v^l_{,x}\right\}\\
N^i_{x\theta} &= \sum_{l=0}^{M}\left\{\frac{1}{R}C^{x\theta21}_{il}u^l_{,\theta}+C^{x\theta22}_{il}v^l_{,x}\right\}\\
Q^i_{xz} &= \sum_{l=0}^{M}\left\{C^{xz11}_{il}u^l\right\}+\sum_{l=0}^{M-1}\left\{C^{xz12}_{il}w^l_{,x}\right\}\\
\bar{Q}^i_{xz} &= \sum_{l=0}^{M}\left\{C^{xz21}_{il}u^l\right\}+\sum_{l=0}^{M-1}\left\{C^{xz22}_{il}w^l_{,x}\right\}\\
Q^i_{\theta z} &= \sum_{l=0}^{M}\left\{C^{\theta z11}_{il}v^l-\frac{1}{R}\hat{C}^{\theta z12}_{il}v^l\right\}+\sum_{l=0}^{M-1}\left\{\frac{1}{R}C^{\theta z12}_{jl}w^l_{,\theta}\right\}\\
\bar{Q}^i_{\theta z} &= \sum_{l=0}^{M}\left\{C^{\theta z21}_{il}v^l-\frac{1}{R}C^{\theta z22}_{il}v^l\right\}+\sum_{l=0}^{M-1}\left\{\frac{1}{R}C^{\theta z22}_{jl}w^l_{,\theta}\right\}
\end{aligned}
\tag{14}
$$

in which cylinder stiffness factors are described using the following formulation

$$
\begin{aligned}
\begin{bmatrix}C^{x11}_{il} & C^{x12}_{il} & C^{x13}_{il}\\ C^{\theta21}_{il} & C^{\theta22}_{il} & C^{\theta23}_{il}\\ C^{z31}_{il} & C^{z32}_{il} & C^{z33}_{il}\end{bmatrix} &= \sum_{k=1}^{N_t}\int_{z_k}^{z_{k+1}}\begin{bmatrix}(1+\frac{z}{R})E^{(k)}_1 & E^{(k)}_2 & \frac{l}{z}(1+\frac{z}{R})E^{(k)}_2\\ E^{(k)}_2 & \frac{1}{(1+\frac{z}{R})}E^{(k)}_1 & \frac{l}{z}E^{(k)}_2\\ \frac{i}{z}(1+\frac{z}{R})E^{(k)}_2 & \frac{i}{z}E^{(k)}_2 & \frac{il}{z^2}(1+\frac{z}{R})E^{(k)}_1\end{bmatrix}z^{i+l}dz\\
\begin{bmatrix}C^{x\theta11}_{il} & C^{x\theta12}_{il}\\ C^{x\theta21}_{il} & C^{x\theta22}_{il}\end{bmatrix} &= \sum_{k=1}^{N_t}\int_{z_k}^{z_{k+1}}\begin{bmatrix}\frac{1}{(1+\frac{z}{R})}E^{(k)}_3 & E^{(k)}_3\\ E^{(k)}_3 & (1+\frac{z}{R})E^{(k)}_3\end{bmatrix}z^{i+l}dz\\
\begin{bmatrix}C^{xz11}_{il} & C^{xz12}_{il}\\ C^{xz21}_{il} & C^{xz22}_{il}\end{bmatrix} &= \sum_{k=1}^{N_t}\int_{z_k}^{z_{k+1}}\begin{bmatrix}\frac{il}{z^2}(1+\frac{z}{R})E^{(k)}_3 & \frac{i}{z}(1+\frac{z}{R})E^{(k)}_3\\ \frac{l}{z}(1+\frac{z}{R})E^{(k)}_3 & (1+\frac{z}{R})E^{(k)}_3\end{bmatrix}z^{i+l}dz\\
\begin{bmatrix}C^{\theta z11}_{il} & C^{\theta z12}_{il}\\ C^{\theta z21}_{il} & C^{\theta z22}_{il}\end{bmatrix} &= \sum_{k=1}^{N_t}\int_{z_k}^{z_{k+1}}\begin{bmatrix}\frac{il}{z^2}(1+\frac{z}{R})E^{(k)}_3 & \frac{i}{z}E^{(k)}_3\\ \frac{l}{z}E^{(k)}_3 & \frac{1}{(1+\frac{z}{R})}E^{(k)}_3\end{bmatrix}z^{i+l}dz
\end{aligned}
\tag{15}
$$

In addition, I_{il} are the inertia terms of structure obtained by

$$
I_{il}=\sum_{k=1}^{N_t}\int_{z_k}^{z_{k+1}}\rho^{(k)}(1+\frac{z}{R})z^{i+l}dz \tag{16}
$$

Substituting Eq. (14) into Eq. (12), the governing motion equations of cylindrical sandwich shell with unconstrained thickness based on the UCHOT are attained in terms of displacements as

$$
\begin{aligned}
&\sum_{l=0}^{M}\left\{C_{il}^{x11}u_{,xx}^{l}+\frac{1}{R^2}C_{il}^{x\theta 11}u_{,\theta\theta}^{l}-C_{il}^{xz11}u^{l}+\frac{1}{R}(C_{il}^{x12}+C_{il}^{x\theta 12})v_{,x\theta}^{l}\right\}\\
&+\sum_{l=0}^{M-1}\left\{(\frac{1}{R}C_{il}^{x12}+C_{il}^{x13}-C_{il}^{xz12})w_{,x}^{l}\right\}=\sum_{l=0}^{M}I_{il}\ddot{u}^{l},\qquad i=0,...,M\\
&\sum_{l=0}^{M}\left\{\frac{1}{R}(C_{il}^{\theta 21}+C_{il}^{x\theta 21})u_{,x\theta}^{l}+\frac{1}{R^2}C_{il}^{\theta 22}v_{,\theta\theta}^{l}+C_{il}^{x\theta 22}v_{,xx}^{l}\right.\\
&\left.+(\frac{1}{R}(C_{il}^{\theta z21}+C_{il}^{\theta z21})-C_{il}^{\theta z11}-\frac{1}{R^2}C_{il}^{\theta z22})v^{l}\right\}\\
&+\sum_{l=0}^{M-1}\left\{\frac{1}{R}(\frac{1}{R}C_{il}^{\theta 22}+C_{il}^{\theta 23}-C_{il}^{\theta z12}+\frac{1}{R}C_{il}^{\theta z22})w_{,\theta}^{l}\right\}=\sum_{l=0}^{M}I_{il}\ddot{v}^{l},\qquad i=0,...,M\\
&\sum_{l=0}^{M}\left\{(C_{jl}^{xz21}-\frac{1}{R}C_{jl}^{\theta 21}-C_{jl}^{z31})u_{,x}^{l}+\frac{1}{R}(C_{jl}^{\theta z21}-\frac{1}{R}C_{jl}^{\theta z22}-\frac{1}{R}C_{jl}^{\theta 22}-C_{jl}^{z32})v_{,\theta}^{l}\right\}\\
&+\sum_{l=0}^{M-1}\left\{C_{jl}^{xz22}w_{,xx}^{l}+\frac{1}{R^2}C_{jl}^{\theta z22}w_{,\theta\theta}^{l}-(C_{jl}^{z33}+\frac{1}{R^2}C_{jl}^{\theta 22}+\frac{1}{R}C_{jl}^{\theta 23}+\frac{1}{R}C_{jl}^{z32})w^{l}\right\}\\
&-\sum_{l=0}^{M-1}(-h/2)^{j+l}(1-\frac{h}{2R})\left\{k_w w^{l}-k_g(w_{,xx}^{l}+\frac{1}{R^2}w_{,\theta\theta}^{l})\right\}=\sum_{l=0}^{M-1}I_{jl}\ddot{w}^{l},\qquad j=0,...,M-1
\end{aligned}
\tag{17}
$$

Furthermore, during the implementing of variational procedure, different boundary conditions of shell for the circular edges ($x=0,L$) can be derived. Major utilized boundary conditions in the analytical and experimental researches are immovable simply supported (S), movable simply supported (MS), clamped (C), and free (F). The mathematically wording of these considering the UCHOT are illustrated as

$$
\begin{aligned}
&\text{for Simply Supported edges (S)}: u^{i,i\neq 2}=N_{xx}^{1}=v^{i}=w^{j}=0\\
&\text{for Movable Simply Supported edges (MS)}: N_{xx}^{i}=v^{i}=w^{j}=0\\
&\text{for Clamped edges (C)}: u^{i}=v^{i}=w^{j}=0\\
&\text{for Free edges (F)}: N_{xx}^{i}=N_{x\theta}^{i}=\bar{Q}_{xz}^{j}+\sum_{l=0}^{M-1}k_g(-h/2)^{j+l}(1-\frac{h}{2R})w_{,x}^{j}=0
\end{aligned}
\tag{18}
$$

where $i=1,2,...,M$ and $j=1,2,...,M$.

5 Solution approach

Using the following approach which is called variable separation in the literature, the dynamic equations (17) for linear treatment of sandwich cylinders can be separated and then solved [74, 75].

$$\left\{ \begin{array}{c} u^i(x,\theta,t) \\ v^i(x,\theta,t) \\ w^j(x,\theta,t) \end{array} \right\} = \sin(\omega t + \alpha') \begin{bmatrix} \sin(n\theta) & 0 & 0 \\ 0 & \cos(n\theta) & 0 \\ 0 & 0 & \sin(n\theta) \end{bmatrix} \left\{ \begin{array}{c} U^i(x) \\ V^i(x) \\ W^j(x) \end{array} \right\} \tag{19}$$

As can be viewed, with selecting the trigonometric terms for the circular direction, the periodicity condition can be satisfied. These terms satisfy kinematic and static conditions at $\theta = 0, 2\pi$. Also, since the free vibration of sandwich shells is harmonic in the time domain, a periodic form can be presumed for the displacement variables, where ω refers to the natural frequency, α' depicts the phase lag, and U^i, V^i, W^j denote the meridional dependent functions (x). Accordingly, n denotes the number of half-wave in the θ axis. Applying the mentioned procedure into the dynamic equations (17), gives (3M+2) coupled x-dependent ordinary differential equations. To achieve an eigenvalue problem, it is necessary to discrete the mentioned ODEs into a system of algebraic equations. To perform this process, generalized differential quadrature (GDQ) method is implemented. This tool is utilized to separate the ODEs in the x-direction [76]. GDQ method is known as an exalted and simple tool and is based on the converting the derivatives of an unknown variable for example $\mathbf{u}$ into a linear summation of weighted coefficients and function values at the defined grid nodes [77, 78]. Application of this tool is represented below for the first and second order derivatives

$$\begin{aligned} \mathbf{u}_{,x}|_{x=x_p} &= \sum_{p'=1}^{N_x} A_{pp'} \mathbf{u}_{p'} \\ \mathbf{u}_{,xx}|_{x=x_p} &= \sum_{p'=1}^{N_x} B_{pp'} \mathbf{u}_{p'} \quad p = 1, 2, ..., N_x \end{aligned} \tag{20}$$

where N_x refers to the number of distributed nodes in the x-direction. Weighted coefficients of the first and second order derivatives are illustrated by $A_{pp'}$ and $B_{pp'}$, respectively, and are determined exploiting the Lagrange interpolated polynomials characterized by the following formula:

$$A_{pp'} = \begin{cases} \frac{\Pi(x_p)}{(x_p - x_{p'})\Pi(x_{p'})} & \text{when} \quad p \neq p' \\ -\sum\limits_{k=1, k\neq p}^{N_x} A_{pk} & \text{when} \quad p = p' \end{cases}, \quad p, p' = 1, 2, ..., N_x \tag{21}$$

in which

$$\Pi(x_p) = \prod_{k=1, k\neq p}^{N_x} (x_p - x_k) \tag{22}$$

and

$$\begin{cases} B_{pp'} = 2\left(A_{pp}A_{pp'} - \frac{A_{pp'}}{(x_p - x_{p'})}\right) & \text{when} \quad p \neq p' \\ B_{pp} = -\sum\limits_{k=1, k\neq p}^{N_x} B_{pk} & \text{when} \quad p = p' \end{cases}, \quad p, p' = 1, 2, ..., N_x \tag{23}$$

The exactitude of GDQ method is severely dependent on the sample of point distribution in the solution field. Chebyshev-Gauss-Lobatto as an effective and accurate node distribution is investigated in the literature [79,80]. The discrete points in the x direction based on this pattern is defined by

$$x_p = L\left(\frac{1}{2} - \frac{1}{2}\cos\left(\frac{p-1}{N_x - 1}\pi\right)\right), \qquad p = 1, 2, \ldots, N_x \tag{24}$$

By engaging Eq. (19) associated GDQ method, both motion equations and boundary conditions turn into an eigenvalue problem related to the free vibration of cylindrical sandwich shells which is not showed here for the sake of brevity. However, to apply this method into the motion equations and also boundary condition one may refer to the available article about this field [73]. The obtained eigenvalue problem may be demonstrated in the compact matrix form as

$$\left(\mathbf{K} - \omega^{\mathbf{2}}\mathbf{M}\right)\mathbf{X} = 0 \tag{25}$$

In Eq. (25), $\mathbf{X}((3M+2)N_x \times 1)$ is the displacement vector, $\mathbf{K}((3M+2)N_x \times (3M+2)N_x)$ refers to the elastic stiffness matrix and $\mathbf{M}$ displays the mass matrix which has $((3M+2)N_x \times (3M+2)N_x)$ components. It should be noticed that a Matlab code is implemented to solve the problem and obtain the natural frequencies corresponding to the circular sandwich cylinders with functionally graded GPLRC face sheets.

6 Numerical results and discussion

The theories and methods mentioned in the previous parts may be used here to probe the free vibration of thick sandwich cylindrical shells on the elastic foundation which consists of a soft core and two FG-GPLRC face sheets. As pointed before, all of the numerical results, layers applied and also GPL weight fraction for both FG-GPLRC face sheets are assumed equal. The shell edges can be clamped (C) or simply supported (S) or free (F) which their mathematical relations are written earlier. The boundary conditions of the cylindrical shell are represented by a two letter brevity, where the first one shows the boundary on $x = 0$ and the second one depicts the boundary on $x = L$. Unless otherwise mentioned, Epoxy is considered as the matrix of composite face sheets and GPLs are considered as nanofillers. Necessary material properties of sandwich constituents are recognized in Table 2. To obtain the effective Young's modulus of the nanocomposite media, Halpin-Tsai's approach is employed. Considering the published experimental paper, the computed theoretical effective Young's modulus employing the Halpin-Tsai model of homogenization and experiments are nearly valid for GPL fillers with the dimensions $a_{GPL} = 2.5\mu$m, $b_{GPL} = 1.5\mu$m, $t_{GPL} = 1.5$nm [81]. As a result, just these sized are exploited for the GPLs in this research.

6.1 Convergence and comparison study

A convergence study is displayed to attain the converged order of displacement series expansion (Eq. (7)) and number of distributed points in the GDQ method (N_x) for free vibration response. For this purpose, fully clamped FG-GPLRC sandwich cylinder with

Table 2: Mechanical properties of the matrix and reinforcement of FG-GPLRC face sheet and core [61, 82].

Properties	Epoxy	GPL	Core
Elasticity modulus (E)[GPa]	3.0	1010	3.0
Mass density (ρ) [kg/m^3]	1200	1062.5	1400
Poisson's ratio (ν)	0.34	0.186	0.4

1% GPL weight fraction for each surface sheet, length-to-radius ratio $L/R = 1$, and $h_f/h = 0.15$ are considered. To develop this study Case2 of functionally graded samples is selected. No elastic foundation is assumed for this example. First four natural frequencies are obtained for different numbers in series expansion and grid points considering two magnitude of thickness-to-radius ration $h/R = 0.1, 0.5$. Numerical outcomes are illustrated in Table (3). Dimensionless frequency parameter is defined as $\Omega_i = \omega_i R\sqrt{\frac{2\rho_c(1+\nu_c)}{E_c}}$. It is found out that the Ninth-order of series expansion ($M = 9$) results in proper accuracy for the first four frequencies. In addition, it can be viewed that the results with $N_x = 15$ has experienced an excellent convergence. Hereupon, $M = 9$ and $N_x = 15$ are assumed for the rest comparison and parametric studies. It should be noticed that the number of laminas for each FG-GPLRC is presumed equal $N_L = 10$. Hence, total number of shell layers is obtained as $N_t = 21$.

Four comparison studies are showed in more forward. As the first comparison, the first ten frequencies in Hertz for an isotropic cylindrical shell with $R = 1$m, $h = 0.1$m, and $L = 2$m is evaluated and collated with the results of Tornabene et al. [77] in Table (4). In the paper [77], natural frequencies of the cylindrical shell are extracted employing the GDQ method based on the first-order shear deformation theory. Material parameters are chosen as $\nu_c = 0.3$, $E = 210$GPa, and $\rho = 7800$kg/m^3. To develop this comparison, the thickness of face sheets is set zero ($h_f = 0$). Three boundary condition types are investigated. A great agreement can be seen between present results and those by Tornabene et al. [77]. This witnessing indicates the efficiency and accuracy of employed unconstrained higher-order theory (UCHOT).

For the second comparison survey, the first three frequencies of a movable simply supported hollow cylinders made of pure/reinforced epoxy with various geometrical factors are examined between present results and those by Liu et al. [51]. Liu et al. [51] investigated the free vibration response using an analytical approach. Three-dimensional elasticity theory is employed to formulate the problem by Liu et al. [51]. GPL is selected to reinforced matrix. To perform this study, GPL weight fraction of total structure is considered $W_{GPL} = 1.5\%$. Geometric parameters are presented in the comparison table. Total number of layers of the employed nanocomposite shell is $N_T = 20$; hence, $N_L = 10$ is considered to investigate the study. Also, the thickness of core is set zero $h_c = 0$. The results are tabulated in Table (5). Uniformly distribution for GPL weight fraction across thickness is considered. Dimensionless frequencies is obtained by $\lambda_i = \omega_i R\sqrt{\frac{\rho_m}{E_m}}$. It should be mentioned that parameter α is defined as $\alpha = m\pi R/L$ where m denotes the number of vibration wave in the longitudinal direction. Mighty agreement can be discerned from this Table (5) that guarantees good accuracy and performance of the employed approach for the shells with arbitrary thickness. In addition, material properties used to perform this study are exactly alike with Table (2). However, mass density of

Table 3: Convergence table of the first four frequencies of cylindrical sandwich shell with Case2 FG pattern.

	Frequency		M				
h/R	Number	N_x	1	3	5	7	9
0.1	Ω_1	9	2.838	2.475	2.467	2.463	2.458
		11	2.838	2.472	2.464	2.460	2.455
		13	2.838	2.471	2.462	2.458	2.453
		15	2.838	2.471	2.461	2.457	2.452
	Ω_2	9	2.892	2.490	2.484	2.480	2.477
		11	2.892	2.487	2.480	2.477	2.473
		13	2.892	2.486	2.479	2.475	2.472
		15	2.892	2.486	2.478	2.475	2.471
	Ω_3	9	3.161	2.728	2.719	2.713	2.708
		11	3.161	2.726	2.716	2.710	2.704
		13	3.161	2.725	2.714	2.709	2.703
		15	3.161	2.725	2.713	2.707	2.702
	Ω_4	9	3.255	2.788	2.781	2.778	2.776
		11	3.255	2.785	2.778	2.776	2.773
		13	3.255	2.785	2.777	2.774	2.772
		15	3.255	2.785	2.776	2.774	2.771
0.5	Ω_1	9	4.455	3.908	3.832	3.811	3.783
		11	4.455	3.908	3.832	3.808	3.780
		13	4.455	3.908	3.832	3.808	3.780
		15	4.455	3.908	3.832	3.807	3.779
	Ω_2	9	4.614	3.926	3.863	3.846	3.823
		11	4.614	3.926	3.862	3.843	3.821
		13	4.614	3.926	3.863	3.843	3.820
		15	4.614	3.926	3.863	3.842	3.820
	Ω_3	9	4.684	4.383	4.294	4.266	4.232
		11	4.684	4.383	4.293	4.263	4.229
		13	4.684	4.383	4.293	4.263	4.229
		15	4.684	4.383	4.293	4.262	4.228
	Ω_4	9	5.272	4.396	4.330	4.311	4.286
		11	5.272	4.396	4.329	4.308	4.283
		13	5.272	4.396	4.329	4.308	4.282
		15	5.272	4.396	4.329	4.307	4.282

GPL is assumed $\rho_{GPL} = 1060\text{kg/m}^3$.

Third comparison study is performed to investigate the validity of the results obtained by the current formulation and those by experimental and three-dimensional elasticity results. For this purpose a hollow cylinder with $L = 254\text{mm}$, $R = 95.25\text{mm}$, and $h = 38.1\text{mm}$ which is a thick structure. Material properties of the cylinder are considered as $E = 207\text{GPa}$, $\rho = 7860\text{kg/m}^3$, and $\nu = 0.28$. The outcomes are tabulated in the Table (6) in which the compared results are taken from a work by [83]. A very good agreement validation is observed that shows the utilized formulation and solution methods are enough effective.

Last comparison study is performed to compare the results attained by the present formulation and those considered the Zig-Zag effects. Also, this example is demonstrated for two hard and soft sandwich structures. For this purpose a parameter FCSR (face-to-core-stiffness ratio) is defined which indicates the ratio of material properties of face respect to core. The results are illustrated in Table (7). In this example, the material

Table 4: Comparison of the frequency (Hz) for an isotropic cylindrical shell ($R = 1$m, $h/a = 0.1$m and $L = 2$m).

CC		SS		CS	
Ref. [77]	Present	Ref. [77]	Present	Ref. [77]	Present
360.36	359.537	331.15	329.200	344.78	343.305
360.36	359.537	331.15	329.200	344.78	343.305
375.86	375.233	348.46	346.875	361.52	360.365
375.86	375.233	348.46	346.875	361.52	360.365
463.29	463.251	440.86	440.024	451.18	450.674
463.29	463.251	440.86	440.024	451.18	450.674
523.55	523.660	508.07	507.890	515.53	515.468
523.55	523.660	508.07	507.890	515.53	515.468
646.56	647.930	596.25	592.664	628.74	625.987
646.56	647.930	596.25	592.664	628.74	625.987

Table 5: Comparison of first three natural frequency parameter $\lambda_i = \omega_i R\sqrt{\frac{\rho_m}{E_m}}$ for a pure epoxy and GPLRC hollow cylinder.

			Pure Epoxy			GPLRC		
Shell Type	α	Source	λ_1	λ_2	λ_3	λ_1	λ_2	λ_3
Thin	2	Ref. [51]	0.1528	0.1588	0.1731	0.3743	0.3891	0.4239
$(\frac{R+h/2}{R-h/2} = 1.01)$		Present	0.1528	0.1588	0.1731	0.3743	0.3891	0.4239
	5	Ref. [51]	0.3850	0.3942	0.4005	0.9429	0.9654	0.9812
		Present	0.3850	0.3942	0.4005	0.9429	0.9654	0.9812
	10	Ref. [51]	0.7747	0.7820	0.7826	1.8976	1.9152	1.9171
		Present	0.7747	0.7820	0.7826	1.8976	1.9152	1.9171
Moderately Thick	2	Ref. [51]	0.9659	0.9996	1.0161	2.3674	2.4499	2.4904
$(\frac{R+h/2}{R-h/2} = 2)$		Present	0.9659	1.0019	1.0161	2.3674	2.4625	2.4904
	5	Ref. [51]	2.6997	2.7156	2.7680	6.6185	6.6576	6.7861
		Present	2.6989	2.7156	2.7680	6.6201	6.6576	6.7861
	10	Ref. [51]	5.6503	5.6603	5.6897	13.8540	13.8785	13.9504
		Present	5.6403	5.6603	5.6897	13.8353	13.8785	13.9504
Thick	2	Ref. [51]	1.1358	1.1386	1.1561	2.7846	2.7916	2.8346
$(\frac{R+h/2}{R-h/2} = 5)$		Present	1.1329	1.1386	1.1561	2.7790	2.7916	2.8346
	5	Ref. [51]	2.8432	2.8458	2.8534	6.9711	6.9773	6.9961
		Present	2.8423	2.8464	2.8541	6.9719	6.9788	6.9976
	10	Ref. [51]	5.6928	5.6940	5.6977	13.9579	13.9610	13.9699
		Present	5.6270	5.7008	5.7372	13.8028	13.9838	14.0667

and geometric properties of the face sheets and core of the structure are exactly the same as in an article by Brischetto et al. [84]. For thick structures, an excellent agreement is seen between the results of this paper with the theory of elasticity and the third-order theory with zigzag effects (EDZ3). Although the results of this paper can be said to be somewhat lower than other theories.

Table 6: Comparison of natural frequencies (Hz) for an isotropic hollow cylinder.

wave number (n)	Source	β_1	β_2
0	Present	8131	8787
	Ref. [83] (Exp)	8109	8817
	Ref. [83](3D)	8149	8886
1	Present	6997	1004
	Ref. [83](Exp)	7104	9859
	Ref. [83] (3D)	7037	9803
2	Present	2547	6390
	Ref. [83] (Exp)	2577	6429
	Ref. [83](3D)	2555	6395
3	Present	6580	9190
	Ref. [83] (Exp)	6618	9210
	Ref. [83](3D)	6592	9232
4	Present	11331	13454
	Ref. [83] (Exp)	11417	13532
	Ref. [83] (3D)	11385	13473
5	Present	16577	18373
	Ref. [83] (Exp)	16597	18390
	Ref. [83] (3D)	16594	18402

Table 7: Comparison of natural frequency parameters $om\bar{e}ga = \omega R^2/h\sqrt{\frac{\rho_{skin}}{E_{skin}}}$ for a sandwich cylindrical shell.

FCSR	R/h	Present	3D [84]	EDZ3 [84]	FSDT [84]
10	10	5.7783	5.7896	5.7937	6.1564
	100	7.3590	7.3593	7.3593	7.3677
	1000	36.525	36.527	36.527	36.528
10^5	10	0.5825	0.6105	0.6742	6.8458
	100	3.9397	3.9470	3.9565	8.0816
	1000	36.550	36.557	36.557	36.678

6.2 Parametric studies

After validating the attained outcomes using the present formulation with the available data from other articles, various parametric researches are tabulated and figured in this segment. Mechanical properties are established from Table (2). For a more perceptible study, natural frequencies have been converted to dimensionless natural frequencies by $\Omega_i = \omega_i R\sqrt{\frac{2\rho_c(1+\nu_c)}{E_c}}$, Winkler parameter becomes dimensionless by $K_W = \frac{k_w R^4 12(1-\nu_c^2)}{E_c H^3}$, and finally Pasternak parameter becomes dimensionless by $K_G = \frac{k_g R^2 12(1-\nu_c^2)}{E_c H^3}$. Results are shown for the first four frequency parameters. It is observed from the available researches, the nanocomposite with $N_L = 10$ is an economical structure (minimum layer) which experiences a smooth stress gradient between laminas. So, number of plies for each FG-GPLRC face sheet is considered equal $N_L = 10$ [61]. Furthermore, from many articles about the GPL-based nanocomposites, GPL weight fraction growth increases the natural frequencies for all cases of functionally grading. Hence, GPL weight fraction of each face nanocomposite plate is assumed $W_{GPL} = 1\%$ in all parametric results. However,

as aforesaid before, according to some laboratory works, excessive increase of graphene causes a sharp decrease in the stiffness of structure, and followed by it a sharp decrease in natural frequencies [23]. In the provided results, the repetitive frequencies are written only once. In all results, the shell radius is equal $R = 1$m.

As a first instance, consider a fully clamped cylindrical sandwich shell with thickness-to-radius ratio $h/R = 0.5$ and length-to-radius ratio $L/R = 1$ without elastic foundation. Table (8) checks out the impact of face sheet thickness h_f on the natural frequencies for the cases of functionally graded patterns. It can be seen that with enlarging the face sheets thickness, the non-dimensional natural frequencies are intelligibly increased. This reason is due to more rigidity of face sheets rather than core. Pure core structure has lowest natural frequency. It is indicated that for sandwich shells, the frequency of shell is largest for FG Case2 rather than other types. When sandwich is made of thin face sheets, Case4 of functionally graded models causes the lowest frequency while the face sheet thickness is grown, this behavior has been changed and sandwich with Case3 has the lowest frequencies. This behavior is due to difference between material properties of sheet and soft core.

Table 8: The influences of face sheet thickness and functionally graded patterns on the first four dimensionless frequency parameters Ω of CC FG-GPLRC cylindrical sandwich shell ($h/R = 0.5$, $L/R = 1$).

h_f/h	FG Case	Ω_1	Ω_2	Ω_3	Ω_4
0.0	1	2.868	2.891	3.142	3.218
	2	2.868	2.891	3.142	3.218
	3	2.868	2.891	3.142	3.218
	4	2.868	2.891	3.142	3.218
	5	2.868	2.891	3.142	3.218
0.05	1	3.231	3.233	3.629	3.646
	2	3.237	3.241	3.636	3.654
	3	3.223	3.224	3.620	3.634
	4	3.216	3.218	3.612	3.623
	5	3.235	3.239	3.636	3.655
0.15	1	3.730	3.780	4.166	4.238
	2	3.779	3.820	4.228	4.282
	3	3.649	3.715	4.066	4.168
	4	3.649	3.718	4.056	4.159
	5	3.715	3.764	4.158	4.233
0.25	1	4.347	4.412	4.832	4.918
	2	4.444	4.491	4.956	5.005
	3	4.145	4.248	4.577	4.740
	4	4.203	4.301	4.632	4.775
	5	4.260	4.334	4.741	4.857
1.0	1	6.517	6.555	7.196	7.219
	2	6.279	6.293	6.941	7.015
	3	6.160	6.202	6.811	6.824
	4	6.408	6.409	7.028	7.065
	5	6.132	6.159	6.816	6.858

To examine the effect of elastic foundation on the natural frequencies of thick sandwich cylinders, Figs. 3,4 are provided. To develop this results, geometrical parameters are considered as $h/R = 0.5$, $L/R = 2$, and $h_f/h = 0.15$. Each figure consists of two subsets,

one for a cylindrical shell with CC boundary conditions and the other with CF boundary conditions. Moreover, Case2 of FG patterns is assumed to perform these examples. It can be observed that appropriate selection of elastic foundation can significantly increase the natural frequencies. Fig. 3 illustrates the effect of dimensionless Pasternak parameter on the first four frequency parameters. In this figure Winkler parameter is assumed zero. It can be seen that the effect of shear layering parameter on each order of frequencies is in a certain range and outside this range has no special effect. For instance, the influence of this factor on the fundamental frequency of CC hollow cylinder is in the range $0 < K_g < 20$. In addition, Fig. 4 gives data about the impact of non-dimensional Winkler parameter on the first four natural frequencies. In this figure Pasternak parameter is assumed zero. The same behavior as seen before can be seen in the effect of this parameter. For example, the influence of Winkler factor on the first natural frequency of CC hollow cylinder is in the range $0 < K_W < 70$

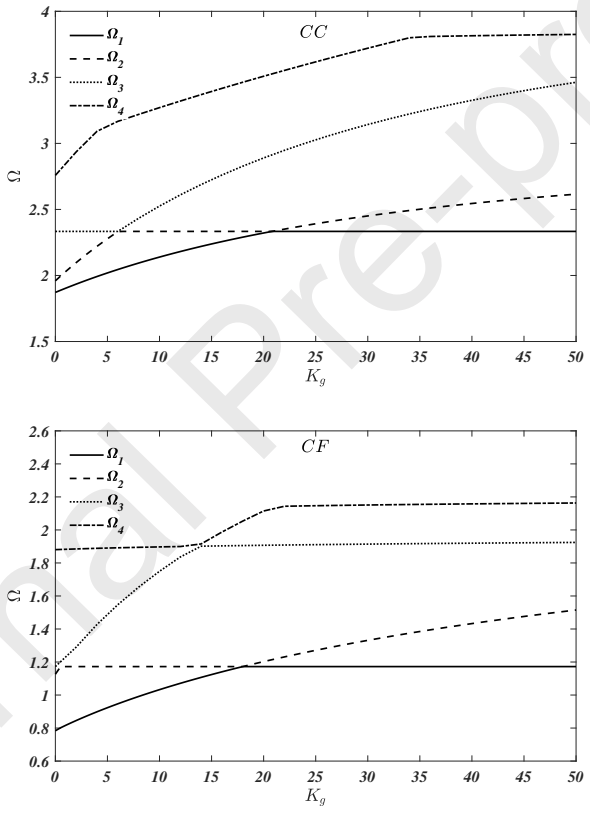

Figure 3: The influence of Pasternak's parameter on the first four dimensionless frequency parameters Ω of FG-GPLRC cylindrical sandwich shell ($h/R = 0.5$, $L/R = 2$, $h_f/h = 0.15$).

Table 9 investigates the impression of length-to-radius ratio L/R and also thickness-to-radius ratio h/R on the frequency response of CC cylindrical shell includes FG-GPLRC face sheets with $h_f/h = 0.15$. Case2 is utilized as reinforce model of face sheets. Beside, two parameters of elastic foundation are supposed equal $(K_W, K_G) = (50, 20)$. At first, it is realized that the cylindrical shell with more length-to-radius ratio, loses its stiffness and therefore its natural frequencies are remarkably decreased. Generally, it is seen that the natural frequencies of shell grows when thickness-to-radius ratio diminishes. However, for

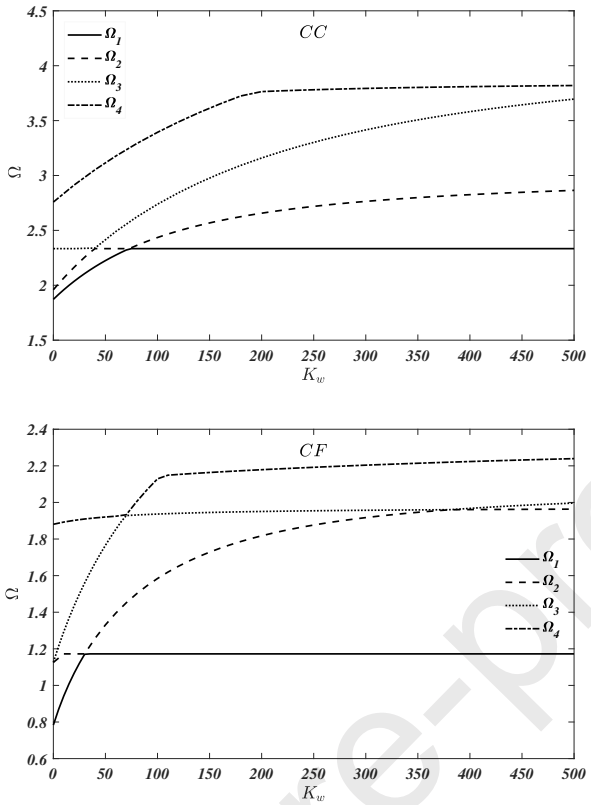

Figure 4: The influence of Winkler's parameter on the first four dimensionless frequency parameters Ω of FG-GPLRC cylindrical sandwich shell ($h/R = 0.5$, $L/R = 2$, $h_f/h = 0.15$).

low values of L/R, there is a critical thickness-to-radius ratio that before it the natural frequencies are enlarged and after that the natural frequencies are reduced with respect to increasing the h/R.

Fig. 5 indicates the frequency behavior of sandwich cylindrical shells with respect to the variation of length-to-radius ratio. This example is prepared for CC and CF shells. Thickness-to-radius ratio and face sheet thickness parameters are respectively considered as $h/R = 0.5$ and $h_f/h = 0.15$. Also, Case2 is elected to locate the GPL weight fraction changes. Moreover, the factors of elastic foundation are presumed as $(K_W, K_G) = (50, 20)$. It can be viewed that with enhancement of L/R, first four natural frequencies of structure decline. This treatment is sharp for the lower amounts of length-to-radius ratio. There is some specific magnitudes of L/R that at its, two consecutive frequencies are equal.

Table 10 explores the power of various boundary conditions on the first four natural frequencies of sandwich shells. This table is provided for circular cylindrical shells with $h/R = 0.5$, $L/R = 1$, and $h_f/h = 0.15$. Case2 of functionally graded is also considered. Elastic foundation with parameters $(K_W, K_G) = (50, 20)$ is located on the inner shell surface. It can be seen that for thick cylindrical shells, the clamped boundary condition has a higher rigidity and is then simply supported and free. Therefore, the shell with clamped conditions has a higher stiffness and consequently a higher natural frequency. It should be distinguished that for completely shell, the zero frequencies are neglected.

Table 9: The influences of L/R and h/R ratios on the first four dimensionless frequency parameters Ω of FG-GPLRC cylindrical sandwich shell ($h_f/h = 0.15$, $(K_W, K_G) = (50, 20)$).

L/R	h/R	Ω_1	Ω_2	Ω_3	Ω_4
0.5	0.2	7.504	7.536	7.601	7.636
	0.4	8.706	8.711	8.823	8.904
	0.8	7.902	7.983	8.190	8.488
	1.0	7.530	7.666	7.973	8.350
1.0	0.2	3.598	3.685	3.886	4.039
	0.4	4.476	4.597	4.648	5.189
	0.8	4.490	4.490	4.656	4.995
	1.0	4.353	4.386	4.476	4.791
2.0	0.2	1.885	1.903	2.309	2.429
	0.4	2.324	2.360	2.830	3.582
	0.8	2.364	2.577	3.113	3.640
	1.0	2.380	2.510	2.888	3.379
4.0	0.2	1.045	1.155	1.310	1.769
	0.4	1.165	1.440	1.932	2.090
	0.8	1.198	1.708	1.919	2.205
	1.0	1.218	1.656	1.894	2.213

These frequencies are related to the rigid body motion.

Table 10: The influences of boundary conditions on the first four dimensionless frequency parameters Ω of FG-GPLRC cylindrical sandwich shell ($h/R = 0.5$, $L/R = 1$, $h_f/h = 0.15$, $(K_W, K_G) = (50, 20)$).

B.Cs	Ω_1	Ω_2	Ω_3	Ω_4
CC	4.583	4.586	4.832	5.360
CS	4.468	4.583	4.691	5.248
CF	2.334	2.437	2.967	3.477
SS	4.400	4.583	4.604	5.169
SF	2.255	2.334	2.796	3.144
FF	0.536	1.190	1.559	2.297

7 Conclusion

In the present research, a natural frequency study for cylindrical sandwich shells made of FG-GPLRC face sheets and soft core is provided. For this purpose, a novel unconstrained higher-order theory is employed for extracting the three dimensional displacements. Material properties of the nanocomposite face sheet are attained utilizing the modified Halpin-Tsai approach which applies the size and geometric of the GPLs in obtaining the elasticity modulus. Hamilton's principle is implemented to form the motion equations of the shell. The governing equations are obtained by means of a semi-analytical procedure based on the GDQ tool. The developed solution technique is employed to attain the natural frequency of arbitrary thickness sandwich shell. It is verified that the

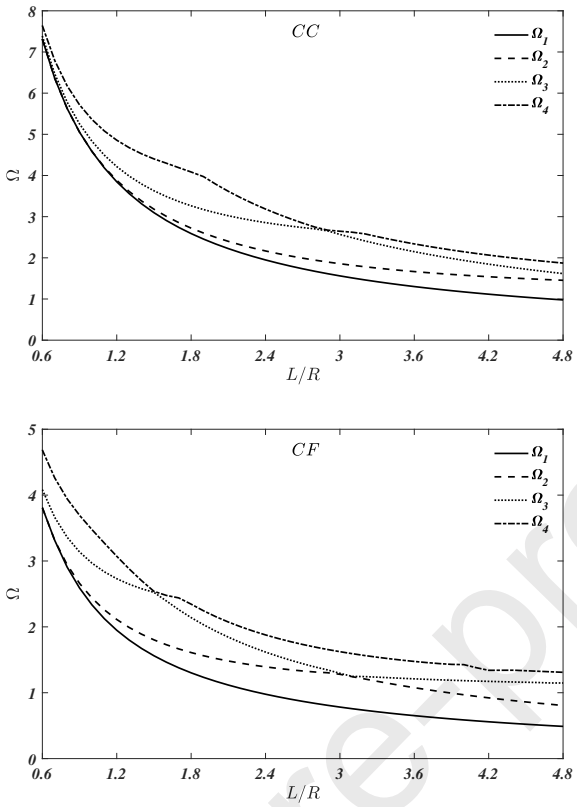

Figure 5: The variation of the first four frequency parameters versus the L/R of the Case2-GPLRC annular sandwich plate for the CC and CF conditions ($h/R = 0.5$, $h_f/h = 0.15$, $(K_W, K_G) = (50, 20)$).

natural frequency parameters based upon the ninth order of displacements expansion are completely valid with those by the three dimensional elasticity theory. Moreover, embedding soft core with the FG-GPLRC sheets outstandingly increases the frequency parameters. Also, it is observed that the functionally graded samples to distribute GPLs has a substantial part to change the frequencies. Case2 and Case5 made sandwich with more frequencies. It is viewed, elastic foundation parameters affect on the shell frequency in a particular range. As expected, the clamped boundary condition hugely increases the flexural rigidity of the structure compared to the others. In addition, the effect of sandwich thickness growth on the natural frequencies, depends on the length-to-radius ratio. In the small range of length-to-radius ratio, there is a critical magnitude for thickness-to-radius ratio that before it, growth of thickness increase frequency parameter but after that the frequencies begin to decrease.

References

[1] Schwingel, D., Seeliger, H.W., Vecchionacci, C., Alwes, D. and Dittrich, J., 2007. Aluminium foam sandwich structures for space applications. *Acta Astronautica*, 61(1-6), pp.326-330.

[2] Shiau, L.C. and Kuo, S.Y., 2006. Free vibration of thermally buckled composite sandwich plates. *Journal of vibration and acoustics*, 128(1), pp.1-7.
[3] Eshaghi, M., 2020. Supersonic flutter analysis of annular/circular sandwich panels containing magnetorheological fluid. *Journal of Sandwich Structures and Materials*, p.1099636220919108.
[4] Dafedar, J.B., Desai, Y.M. and Mufti, A.A., 2003. Stability of sandwich plates by mixed, higher-order analytical formulation. *International journal of solids and structures*, 40(17), pp.4501-4517.
[5] Zenkour, A.M. and Radwan, A.F., 2018. Free vibration analysis of multilayered composite and soft core sandwich plates resting on WinklerPasternak foundations. *Journal of Sandwich Structures and Materials*, 20(2), pp.169-190.
[6] Torabi, J., Ansari, R. and Hasrati, E., 2020. Mechanical buckling analyses of sandwich annular plates with functionally graded carbon nanotube-reinforced composite face sheets resting on elastic foundation based on the higher-order shear deformation plate theory. *Journal of Sandwich Structures and Materials*, 22(6), pp.1812-1837.
[7] Manh, D.T., Anh, V.T.T., Nguyen, P.D. and Duc, N.D., 2020. Nonlinear post-buckling of CNTs reinforced sandwich-structured composite annular spherical shells. *International Journal of Structural Stability and Dynamics*, 20(02), p.2050018.
[8] Xia, X.K. and Shen, H.S., 2008. Vibration of post-buckled sandwich plates with FGM face sheets in a thermal environment. *Journal of Sound and Vibration*, 314(1-2), pp.254-274.
[9] Meksi, R., Benyoucef, S., Mahmoudi, A., Tounsi, A., Adda Bedia, E.A. and Mahmoud, S.R., 2019. An analytical solution for bending, buckling and vibration responses of FGM sandwich plates. *Journal of Sandwich Structures and Materials*, 21(2), pp.727-757.
[10] Bourada, M., Tounsi, A., Houari, M.S.A. and Bedia, E.A.A., 2012. A new four-variable refined plate theory for thermal buckling analysis of functionally graded sandwich plates. *Journal of Sandwich Structures and Materials*, 14(1), pp.5-33.
[11] Arshid, E., Amir, S. and Loghman, A., 2020. Bending and buckling behaviors of heterogeneous temperature-dependent micro annular/circular porous sandwich plates integrated by FGPEM nano-Composite layers. *Journal of Sandwich Structures and Materials*, p.1099636220955027.
[12] Reddy, C.D., Rajendran, S. and Liew, K.M., 2006. Equilibrium configuration and continuum elastic properties of finite sized graphene. *Nanotechnology*, 17(3), p.864.
[13] Scarpa, F., Adhikari, S. and Phani, A.S., 2009. Effective elastic mechanical properties of single layer graphene sheets. *Nanotechnology*, 20(6), p.065709.
[14] Cadelano, E., Palla, P.L., Giordano, S. and Colombo, L., 2009. Nonlinear elasticity of monolayer graphene. *Physical review letters*, 102(23), p.235502.
[15] Ni, Z., Bu, H., Zou, M., Yi, H., Bi, K. and Chen, Y., 2010. Anisotropic mechanical properties of graphene sheets from molecular dynamics. *Physica B: Condensed Matter*, 405(5), pp.1301-1306.
[16] Zhang, Y.Y., Wang, C.M., Cheng, Y. and Xiang, Y., 2011. Mechanical properties of bilayer graphene sheets coupled by sp3 bonding. *Carbon*, 49(13), pp.4511-4517.
[17] Rafiee, M.A., Rafiee, J., Wang, Z., Song, H., Yu, Z.Z. and Koratkar, N., 2009. Enhanced mechanical properties of nanocomposites at low graphene content. *ACS nano*, 3(12), pp.3884-3890.
[18] Zhao, X., Zhang, Q., Chen, D. and Lu, P., 2010. Enhanced mechanical properties of graphene-based poly (vinyl alcohol) composites. *Macromolecules*, 43(5), pp.2357-

2363.

[19] King, J.A., Klimek, D.R., Miskioglu, I. and Odegard, G.M., 2013. Mechanical properties of graphene nanoplatelet/epoxy composites. *Journal of applied polymer science*, 128(6), pp.4217-4223.

[20] Fang, M., Wang, K., Lu, H., Yang, Y. and Nutt, S., 2009. Covalent polymer functionalization of graphene nanosheets and mechanical properties of composites. *Journal of Materials Chemistry*, 19(38), pp.7098-7105.

[21] Song, M., Kitipornchai, S. and Yang, J., 2017. Free and forced vibrations of functionally graded polymer composite plates reinforced with graphene nanoplatelets. *Composite Structures*, 159, pp.579-588.

[22] Chandra, Y., Chowdhury, R., Scarpa, F., Adhikari, S., Sienz, J., Arnold, C., Murmu, T. and Bould, D., 2012. Vibration frequency of graphene based composites: a multiscale approach. *Materials Science and Engineering: B*, 177(3), pp.303-310.

[23] Kulkarni, D.D., Choi, I., Singamaneni, S.S. and Tsukruk, V.V., 2010. Graphene oxide polyelectrolyte nanomembranes. *ACS nano*, 4(8), pp.4667-4676.

[24] Kitipornchai, S., Chen, D. and Yang, J., 2017. Free vibration and elastic buckling of functionally graded porous beams reinforced by graphene platelets. *Materials and Design*, 116, pp.656-665.

[25] Song, M., Gong, Y., Yang, J., Zhu, W. and Kitipornchai, S., 2019. Free vibration and buckling analyses of edge-cracked functionally graded multilayer graphene nanoplatelet-reinforced composite beams resting on an elastic foundation. *Journal of Sound and Vibration*, 458, pp.89-108.

[26] Wang, Y., Feng, C., Wang, X., Zhao, Z., Romero, C.S., Dong, Y. and Yang, J., 2019. Nonlinear static and dynamic responses of graphene platelets reinforced composite beam with dielectric permittivity. *Applied Mathematical Modelling*, 71, pp.298-315.

[27] Barati, M.R. and Shahverdi, H., 2020. Finite element forced vibration analysis of refined shear deformable nanocomposite graphene platelet-reinforced beams. *Journal of the Brazilian Society of Mechanical Sciences and Engineering*, 42(1), p.33.

[28] Wang, Y., Xie, K., Fu, T. and Shi, C., 2019. Vibration response of a functionally graded graphene nanoplatelet reinforced composite beam under two successive moving masses. *Composite Structures*, 209, pp.928-939.

[29] Li, X., Song, M., Yang, J. and Kitipornchai, S., 2019. Primary and secondary resonances of functionally graded graphene platelet-reinforced nanocomposite beams. *Nonlinear Dynamics*, 95(3), pp.1807-1826.

[30] Feng, C., Kitipornchai, S. and Yang, J., 2017. Nonlinear free vibration of functionally graded polymer composite beams reinforced with graphene nanoplatelets (GPLs). *Engineering Structures*, 140, pp.110-119.

[31] Yang, J., Chen, D. and Kitipornchai, S., 2018. Buckling and free vibration analyses of functionally graded graphene reinforced porous nanocomposite plates based on Chebyshev-Ritz method. *Composite Structures*, 193, pp.281-294.

[32] Reddy, R.M.R., Karunasena, W. and Lokuge, W., 2018. Free vibration of functionally graded-GPL reinforced composite plates with different boundary conditions. *Aerospace Science and Technology*, 78, pp.147-156.

[33] Zhao, Z., Feng, C., Wang, Y. and Yang, J., 2017. Bending and vibration analysis of functionally graded trapezoidal nanocomposite plates reinforced with graphene nanoplatelets (GPLs). *Composite Structures*, 180, pp.799-808.

[34] Guo, H., Cao, S., Yang, T. and Chen, Y., 2018. Vibration of laminated composite quadrilateral plates reinforced with graphene nanoplatelets using the element-free

IMLS-Ritz method. *International Journal of Mechanical Sciences*, 142, pp.610-621.

[35] Gholami, R. and Ansari, R., 2018. Nonlinear harmonically excited vibration of third-order shear deformable functionally graded graphene platelet-reinforced composite rectangular plates. *Engineering Structures*, 156, pp.197-209.

[36] Malekzadeh, P., Setoodeh, A.R. and Shojaee, M., 2018. Vibration of FG-GPLs eccentric annular plates embedded in piezoelectric layers using a transformed differential quadrature method. *Computer Methods in Applied Mechanics and Engineering*, 340, pp.451-479.

[37] Saidi, A.R., Bahaadini, R. and Majidi-Mozafari, K., 2019. On vibration and stability analysis of porous plates reinforced by graphene platelets under aerodynamical loading. *Composites Part B: Engineering*, 164, pp.778-799.

[38] Selim, B.A., Liu, Z. and Liew, K.M., 2019. Active vibration control of functionally graded graphene nanoplatelets reinforced composite plates integrated with piezoelectric layers. *Thin-Walled Structures*, 145, p.106372.

[39] Wang, Y., Zeng, R. and Safarpour, M., 2020. Vibration analysis of FG-GPLRC annular plate in a thermal environment. *Mechanics Based Design of Structures and Machines*, pp.1-19.

[40] Gholami, R. and Ansari, R., 2019. Nonlinear stability and vibration of pre/post-buckled multilayer FG-GPLRPC rectangular plates. *Applied Mathematical Modelling*, 65, pp.627-660.

[41] Gholami, R. and Ansari, R., 2019. On the nonlinear vibrations of polymer nanocomposite rectangular plates reinforced by graphene nanoplatelets: a unified higher-order shear deformable model. *Iranian Journal of Science and Technology, Transactions of Mechanical Engineering*, 43(1), pp.603-620.

[42] Liu, D., Li, Z., Kitipornchai, S. and Yang, J., 2019. Three-dimensional free vibration and bending analyses of functionally graded graphene nanoplatelets-reinforced nanocomposite annular plates. Composite Structures, 229, p.111453.

[43] Dong, Y.H., Li, Y.H., Chen, D. and Yang, J., 2018. Vibration characteristics of functionally graded graphene reinforced porous nanocomposite cylindrical shells with spinning motion. *Composites Part B: Engineering*, 145, pp.1-13.

[44] Dong, Y.H., Zhu, B., Wang, Y., Li, Y.H. and Yang, J., 2018. Nonlinear free vibration of graded graphene reinforced cylindrical shells: Effects of spinning motion and axial load. *Journal of Sound and Vibration*, 437, pp.79-96.

[45] Barati, M.R. and Zenkour, A.M., 2018. Vibration analysis of functionally graded graphene platelet reinforced cylindrical shells with different porosity distributions. *Mechanics of Advanced Materials and Structures*, pp.1-9.

[46] Heydarpour, Y., Mohammadzaheri, M., Ghodsi, M., Soltani, P., AlJahwari, F., Bahadur, I. and Al-Amri, B., 2020. Application of the hybrid DQ-Heaviside-NURBS method for dynamic analysis of FG-GPLRC cylindrical shells subjected to impulse load. *Thin-Walled Structures*, 155, p.106914.

[47] Wang, Y.Q., Ye, C. and Zu, J.W., 2019. Nonlinear vibration of metal foam cylindrical shells reinforced with graphene platelets. *Aerospace Science and Technology*, 85, pp.359-370.

[48] Niu, Y., Zhang, W. and Guo, X.Y., 2019. Free vibration of rotating pretwisted functionally graded composite cylindrical panel reinforced with graphene platelets. *European Journal of Mechanics-A/Solids*, 77, p.103798.

[49] Wang, A., Chen, H., Hao, Y. and Zhang, W., 2018. Vibration and bending behavior of functionally graded nanocomposite doubly-curved shallow shells reinforced by

graphene nanoplatelets. *Results in Physics*, 9, pp.550-559.

[50] Bidzard, A., Malekzadeh, P. and Mohebpour, S.R., 2019. Vibration of multilayer FG-GPLRC toroidal panels with elastically restrained against rotation edges. *Thin-Walled Structures*, 143, p.106209.

[51] Liu, D., Kitipornchai, S., Chen, W. and Yang, J., 2018. Three-dimensional buckling and free vibration analyses of initially stressed functionally graded graphene reinforced composite cylindrical shell. *Composite Structures*, 189, pp.560-569.

[52] Samaniego, E., Anitescu, C., Goswami, S., Nguyen-Thanh, V.M., Guo, H., Hamdia, K., Zhuang, X. and Rabczuk, T., 2020. An energy approach to the solution of partial differential equations in computational mechanics via machine learning: Concepts, implementation and applications. *Computer Methods in Applied Mechanics and Engineering*, 362, p.112790.

[53] Vu-Bac, N., Duong, T.X., Lahmer, T., Zhuang, X., Sauer, R.A., Park, H.S. and Rabczuk, T., 2018. A NURBS-based inverse analysis for reconstruction of nonlinear deformations of thin shell structures. *Computer Methods in Applied Mechanics and Engineering*, 331, pp.427-455.

[54] Nguyen-Thanh, N., Zhou, K., Zhuang, X., Areias, P., Nguyen-Xuan, H., Bazilevs, Y. and Rabczuk, T., 2017. Isogeometric analysis of large-deformation thin shells using RHT-splines for multiple-patch coupling. *Computer Methods in Applied Mechanics and Engineering*, 316, pp.1157-1178.

[55] Anitescu, C., Atroshchenko, E., Alajlan, N. and Rabczuk, T., 2019. Artificial neural network methods for the solution of second order boundary value problems. *Computers, Materials and Continua*, 59(1), pp.345-359.

[56] Rabczuk, T., Areias, P.M.A. and Belytschko, T., 2007. A meshfree thin shell method for nonlinear dynamic fracture. *International journal for numerical methods in engineering*, 72(5), pp.524-548.

[57] Tornabene, F., Fantuzzi, N. and Bacciocchi, M., 2016. The GDQ method for the free vibration analysis of arbitrarily shaped laminated composite shells using a NURBS-based isogeometric approach. *Composite Structures*, 154, pp.190-218.

[58] Nematollahi, M.S., Mohammadi, H., Dimitri, R. and Tornabene, F., 2020. Nonlinear Vibration of Functionally Graded Graphene Nanoplatelets Polymer Nanocomposite Sandwich Beams. *Applied Sciences*, 10(16), p.5669.

[59] Liang, D., Wu, Q., Lu, X. and Tahouneh, V., 2020. Vibration behavior of trapezoidal sandwich plate with functionally graded-porous core and graphene platelet-reinforced layers. *Steel and Composite Structures*, 36(1), pp.47-62.

[60] Mohseni, A. and Shakouri, M., 2020. Natural frequency, damping and forced responses of sandwich plates with viscoelastic core and graphene nanoplatelets reinforced face sheets. *Journal of Vibration and Control*, p.1077546319893453.

[61] Javani, M., Kiani, Y. and Eslami, M.R., 2020. Thermal buckling of FG graphene platelet reinforced composite annular sector plates. *Thin-Walled Structures*, 148, p.106589.

[62] Rissanou, A.N., Power, A.J. and Harmandaris, V., 2015. Structural and dynamical properties of polyethylene/graphene nanocomposites through molecular dynamics simulations. *Polymers*, 7(3), pp.390-417.

[63] Affdl, J.H. and Kardos, J.L., 1976. The HalpinTsai equations: a review. *Polymer Engineering and Science*, 16(5), pp.344-352.

[64] Love, A.E.H., 1888. XVI. The small free vibrations and deformation of a thin elastic shell. *Philosophical Transactions of the Royal Society of London.(A.)*, (179), pp.491-

546.

[65] E. Reissner, The Effect of Transverse Shear Deformation on the Bending of Elastic Plates, *Journal of applied mechanics*, 12 (1945), pp. 69-77.

[66] Reddy, J., 1984. A simple higher-order theory for laminated composite plates. *Journal of applied mechanics*, 51(4), pp.745-752.

[67] Sayyad, A.S. and Ghugal, Y.M., 2019. Static and free vibration analysis of laminated composite and sandwich spherical shells using a generalized higher-order shell theory. Composite Structures, 219, pp.129-146.

[68] Natarajan, S., Haboussi, M. and Manickam, G., 2014. Application of higher-order structural theory to bending and free vibration analysis of sandwich plates with CNT reinforced composite facesheets. Composite Structures, 113, pp.197-207.

[69] Matsunaga, H., 1992. The application of a two-dimensional higher-order theory for the analysis of a thick elastic plate. *Computers and structures*, 45(4), pp.633-648.

[70] Matsunaga, H., 2007. Vibration and buckling of cross-ply laminated composite circular cylindrical shells according to a global higher-order theory. *International journal of mechanical sciences*, 49(9), pp.1060-1075.

[71] Matsunaga, H., 2009. Free vibration and stability of functionally graded circular cylindrical shells according to a 2D higher-order deformation theory. *Composite Structures*, 88(4), pp.519-531.

[72] Sahraee, S. and Saidi, A.R., 2009. Free vibration and buckling analysis of functionally graded deep beam-columns on two-parameter elastic foundations using the differential quadrature method. *Proceedings of the Institution of Mechanical Engineers, Part C: Journal of Mechanical Engineering Science*, 223(6), pp.1273-1284.

[73] Javani, M., Kiani, Y. and Eslami, M.R., 2019. Free vibration of arbitrary thick FGM deep arches using unconstrained higher-order shear deformation theory. *Thin-Walled Structures*, 136, pp.258-266.

[74] M. Mirzaei, Y. Kiani, Thermal buckling of temperature dependent FG-CNT reinforced composite conical shells, *Aerospace Science and Technology*, 47, pp.42-53, 2015.

[75] Soureshjani, A.H., Talebitooti, R. and Talebitooti, M., A semi-analytical approach on the effect of external lateral pressure on free vibration of joined sandwich aerospace composite conical-conical shells, *Aerospace Science and Technology*, 99, p.105559, 2020.

[76] Javani, M., Kiani, Y. and Eslami, M.R., 2019. Large amplitude thermally induced vibrations of temperature dependent annular FGM plates. *Composites Part B: Engineering*, 163, pp.371-383.

[77] Tornabene, F., Viola, E. and Inman, D.J., 2009. 2-D differential quadrature solution for vibration analysis of functionally graded conical, cylindrical shell and annular plate structures. *Journal of Sound and Vibration*, 328(3), pp.259-290.

[78] Javani, M., Kiani, Y., Sadighi, M. and Eslami, M.R., 2019. Nonlinear vibration behavior of rapidly heated temperature-dependent FGM shallow spherical shells. *AIAA Journal*, 57(9), pp.4071-4084.

[79] Tornabene, F., 2009. Free vibration analysis of functionally graded conical, cylindrical shell and annular plate structures with a four-parameter power-law distribution. *Computer Methods in Applied Mechanics and Engineering*, 198(37-40), pp.2911-2935.

[80] Javani, M., Kiani, Y. and Eslami, M.R., 2019. Nonlinear axisymmetric response of temperature-dependent FGM conical shells under rapid heating. Acta Mechanica, 230(9), pp.3019-3039.

[81] Rafiee, M.A., Graphene-based composite materials. *Rensselaer Polytechnic Institute: Troy, NY, USA*, 2011.

[82] Brischetto, S., 2013. Hygrothermoelastic analysis of multilayered composite and sandwich shells. *Journal of Sandwich Structures and Materials*, 15(2), pp.168-202.

[83] So, J. and Leissa, A., 1997. Free vibrations of thick hollow circular cylinders from three-dimensional analysis. *Journal of vibration and acoustics*, 119(1), pp.89-95.

[84] Brischetto, S., Carrera, E. and Demasi, L., 2009. Free vibration of sandwich plates and shells by using zig-zag function. *Shock and Vibration*, 16(5), pp.495-503.